Delft University of Technology

Numerical and Experimental Investigation of the Mitigation of Landing Gear Noise Using Diamond Lattice Fairings

Li, Shuai; Davidson, Lars ; Peng, Shia-Hui ; Rubio Carpio, A.; Ragni, D.; Avallone, F.

Citation (APA)
Li, S., Davidson, L., Peng, S.-H., Rubio Carpio, A., Ragni, D., & Avallone, F. (2024). Numerical and Experimental Investigation of the Mitigation of Landing Gear Noise Using Diamond Lattice Fairings. In *30th AIAA/CEAS Aeroacoustics Conference (2024)* Article AIAA 2024-3283 (30th AIAA/CEAS Aeroacoustics Conference, 2024). https://doi.org/10.2514/6.2024-3283

Important note
To cite this publication, please use the final published version (if applicable).
Please check the document version above.

Check for updates

Numerical and Experimental Investigation of the Mitigation of Landing Gear Noise using Diamond Lattice Fairings

Shuai Li [*], Lars Davidson[†], Shia-Hui Peng [‡]
Chalmers University of Technology, SE-412 96 Gothenburg, Sweden

Alejandro Rubio Carpio[§], Daniele Ragni[¶]
Delft University of Technology, Kluyverweg 1, 2629 HS Delft, The Netherlands

Francesco Avallone[‖]
Politecnico di Torino, Corso Duca degli Abruzzi 24, 10122, Torino, Italy

Two passive add-on porous fairings, comprised of diamond grids varying in size, are numerically and experimentally investigated for their effectiveness in mitigating landing gear noise. The baseline landing gear, a modified version of the LAGOON landing gear with its inner rim cavities closed, along with two configurations equipped with diamond-lattice fairings, are numerically simulated using the Improved Delayed Detached-Eddy Simulation (IDDES) in combination with the Ffowcs Williams and Hawkings (FW-H) analogy. Instead of resolving the detailed flow features through the diamond-lattice fairings, a numerical model is employed to represent the effect of fairing. Prior to integrating the numerical model into the simulations of landing gears, rigorous validation of the model against experimental data in a channel flow is performed. Subsequently, the predicted flow fields and far-field noise spectra of the baseline and controlled landing gears are validated against the experiments conducted in the anechoic A-Tunnel at Delft University of Technology. The results indicate that implementing a diamond-lattice fairing upstream of the landing gear can effectively diminish far-field noise in the frequency range exceeding 200 Hz. For the baseline landing gear, the torque link and brakes are potent noise sources. For the controlled landing gears, both diamond-lattice fairings mitigate the pressure fluctuations on the torque link and brakes, leading to a reduction of surface noise sources. The noise directivity shows that the DL 4.5mm fairing produces a noise reduction of 2-6 dB whereas the DL 2.5mm fairing generates a noise reduction of 3-7 dB across all radial directions. These findings pave the way for the low-noise design of aircraft landing gears.

Nomenclature

C_p	=	pressure coefficient
d_c	=	size of diamond grids, mm
d_w	=	wheel diameter of the landing gears, m
Δt	=	time step, s
Δx_{min}	=	minimum streamwise grid size, mm
$\Delta x_{max,u}$	=	maximum streamwise grid size in the upstream mesh block, mm
$\Delta x_{max,d}$	=	maximum streamwise grid size in the downstream mesh block, mm
Δy	=	grid size in y direction, mm
Δz	=	grid size in z direction, mm
f	=	frequency of sound, Hz

[*]Postdoctoral researcher, Department of Mechanics and Maritime Sciences, shuai.li@chalmers.se.

[†]Professor, Department of Mechanics and Maritime Sciences, lars.davidson@chalmers.se.

[‡]Guest Professor, Department of Mechanics and Maritime Sciences, peng@chalmers.se, AIAA Associate Fellow.

[§]Doctor, Faculty of Aerospace Engineering, alrucar1@gmail.com.

[¶]Associate Professor, Faculty of Aerospace Engineering, d.ragni@tudelft.nl, AIAA member.

[‖]Professor, Department of Mechanical and Aerospace Engineering, francesco.avallone@polito.it, AIAA member.

H	=	height of fairing, m
h	=	thickness of the source region, m
K_0	=	resistance coefficient at normal incidence
L	=	width of fairing, m
ω	=	specific rate of dissipation, s^{-1}
$\hat{p}$	=	pressure, Pa
p_{ref}	=	reference pressure, Pa
p'_{rms}	=	root-mean-square pressure fluctuation, Pa
ρ	=	density, kg/m^3
$\hat{\sigma}_{ij}$	=	viscous stress tensor, kg/m/s^2
$\sigma_{ij,model}$	=	modelled stress tensor, kg/m/s^2
$SPL_{1/3}$	=	1/3-octave bin-averaged Sound Pressure Level, dB
θ	=	angular coordinate, degree
U_0	=	free-stream velocity of flow past landing gears, m/s
U'	=	turbulent intensity, m/s
u_0	=	inlet velocity of channel flow, m/s
$\hat{u}_i$	=	components of velocity (i=1, 2, 3), m/s
$\bar{u}$	=	mean streamwise velocity, m/s
u'	=	root-mean-square of streamwise velocity fluctuation, m/s
$\bar{v}$	=	mean lateral velocity, m/s
v'	=	root-mean-square of lateral velocity fluctuation, m/s
$\bar{w}$	=	mean vertical velocity, m/s
w'	=	root-mean-square of vertical velocity fluctuation, m/s
$x_{fairing}$	=	streamwise position of fairing, m
DL	=	diamond lattice
FOV	=	field of view
FW-H	=	Ffowcs Williams and Hawkings
IDDES	=	Improved Delayed Detached-Eddy Simulation
LES	=	large-eddy simulation
LG	=	landing gear
OASPL	=	Overall Sound Pressure Level, dB
PIV	=	Particle Image Velocimetry
RANS	=	Reynolds-averaged Navier–Stokes
SPL	=	Sound Pressure Level, dB

I. Introduction

Aircraft landing gear (LG) noise is a significant contributor to airframe noise produced during take-off, approach and landing phases of an aircraft. During such phases, the landing gear interacts with the airflow, producing aerodynamic noise that can be perceived in the vicinity of airports. The LG noise is mainly generated by (i) flow separation off different individual structural components (wheels, brakes, torque links, axles, bogies and sidestays, etc) and (ii) the interaction of turbulent wakes from upstream components with downstream structural components [1]. Understanding and mitigating aircraft landing gear noise is crucial not only for meeting regulatory noise standards but also for enhancing the comfort of passengers and minimizing the environmental impact of aviation operations.

Over the past two decades, numerous studies have shown that add-on fairings can be a promising technological solution for reducing LG noise [2–6]. Initially, solid fairings were introduced for this purpose. However, a major drawback of solid fairings is that the impinging flow can be deflected to adjacent and downstream components, thereby enhancing the interaction between the turbulent wake and downstream components [5]. Furthermore, in comparison to porous fairings, flow velocity towards the sides of a solid fairing is notably higher [5], leading to larger-scale flow separation and increasing aerodynamic drag. Contrary to solid fairings, porous fairings offer a key advantage in that they diminish flow deflection towards the fairing sides by facilitating mass flux through their pores, potentially resulting in reduced aerodynamic drag.

In the present study, we numerically and experimentally investigate two passive add-on porous fairings consisting of diamond lattices of 2.5 mm and 4.5 mm in size (hereinafter referred to as DL 2.5mm and DL 4.5mm, respectively) for
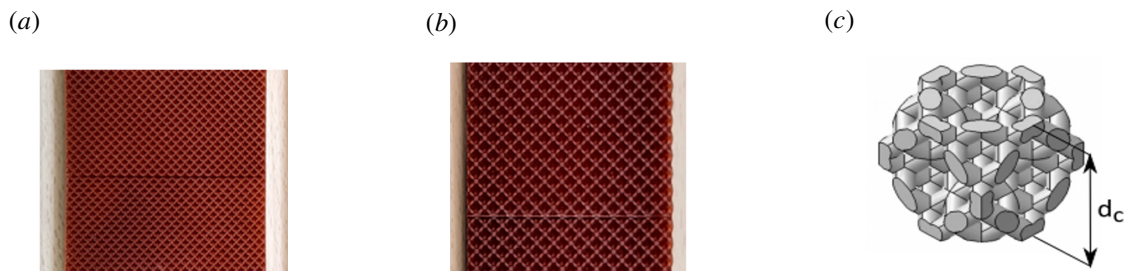
2

Fig. 1 Two porous fairings consisting of diamond grids of 2.5 mm and 4.5 mm in size: (a) 2.5 mm; (b) 4.5 mm; and (c) definition of the diamond grid size d_c.
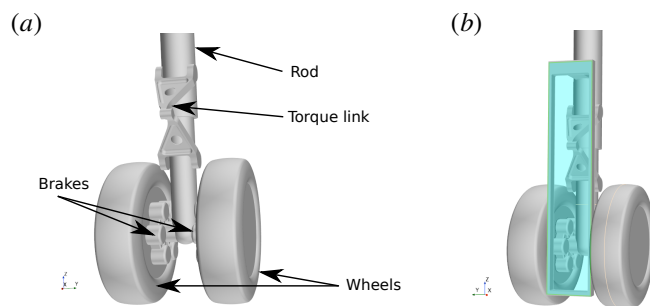

Fig. 2 The LAGOON-like landing gear: (a) Baseline configuration; and (b) controlled configuration equipped with a porous fairing.

LG noise reduction. These diamond-lattice fairings have been designed and manufactured by Trinity College Dublin [6] and are shown in Figure 1. The turbulent flows over a baseline landing gear, a modified version of the LAGOON landing gear with its inner rim cavities closed in order to avoid the Rossiter instabilities [7], along with two configurations equipped with diamond-lattice fairings, are simulated using IDDES in conjunction with the FW-H analogy for acoustic analysis. Both the baseline and controlled LG configurations are shown in Figure 2.

The paper is organized as follows: Section II provides a detailed description of the experimental set-up, numerical method, numerical set-up for the simulations of landing gears, and the fairing model for the controlled LG equipped with diamond-lattice fairings. Rigorous validation of the fairing model against experimental data in a channel flow is performed in Section III. Aerodynamic and acoustic results pertaining to experimental measurements and numerical simulations of the landing gears are presented in Section IV. Finally, Section V offers concluding remarks summarizing the key findings.

II. Experiments and numerical methods

A. Experimental set-up

The measured flow data and acoustic spectra of the LAGOON-like landing gear, which will be used to validate the present numerical simulations, are acquired in the A-Tunnel of the Delft University of Technology [6, 8–10]. The A-Tunnel is a vertical wind tunnel characterized by an open-jet, closed-circuit design. Its open-jet test section is housed within an anechoic room measuring $6.4 \times 6.4 \times 3.2 \, \text{m}^3$ in dimensions. Flamex acoustic absorbing foam wedges cover the walls and ceiling of the anechoic room to prevent undesirable sound reflections. The vertical nozzle features a rectangular exit measuring $400 \times 700 \, \text{mm}^2$, as illustrated in Figure 3. Figure 4(a) illustrates two microphone measurement configurations, both utilizing a single microphone array. In the "flyover" configuration, the array is positioned at the bottom of the LG, while in the "sideline" configuration, it is placed laterally. The microphone array comprises 64 GRAS 40PH analog free-field microphones with integrated constant current power amplifiers. These 64 microphones
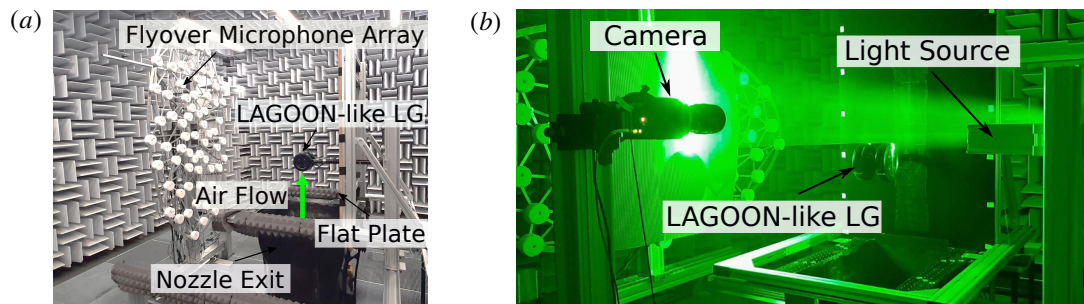
Fig. 3 Experimental setup in the A-Tunnel of Delft University of Technology: (a) Microphone measurement; and (b) PIV measurement.
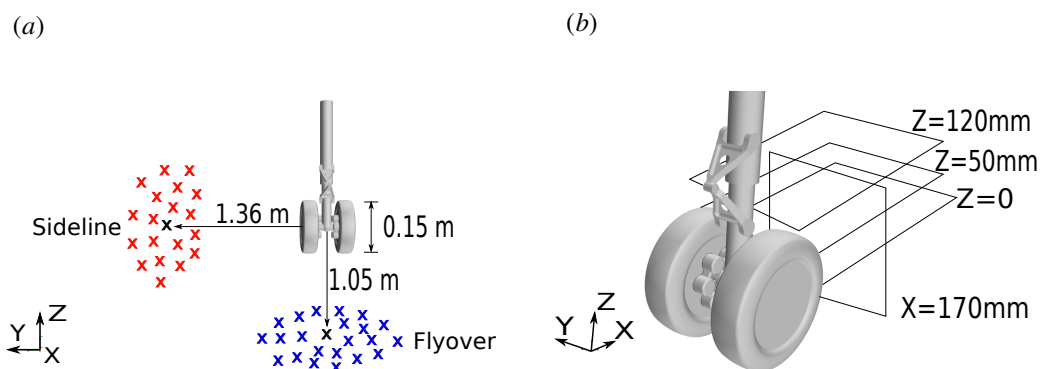

Fig. 4 Microphone and PIV measurements: (a) Sideline (in red) and flyover (in blue) microphone configurations. The microphone array consists of 64 microphones with the center microphone highlighted in black color; and (b) a sketch of four planes downstream of a landing gear where flow fields are measured using PIV.

are arranged over a planar ellipse with a major-to-minor axis ratio of 2 and a major effective diameter of 2 m [9]. In the flyover configuration, the center microphone is positioned at coordinates $(X, Y, Z) = (0.22, -0.02, -1.05)$ m, where X, Y, and Z represent the streamwise, lateral, and vertical directions, respectively. For the sideline configuration, the center microphone is located at $(0.22, 1.36, 0)$ m. The origin of the coordinate system is situated at the point where the axis of the LG axle intersects with the axis of the rod connecting the two wheels. The diameter of the LG wheels is $d_w = 150$ mm. In all the acoustic measurements conducted in the present study, a recording duration of 20 s and a sampling frequency of 51.2 kHz are adopted. The spectra of the acoustic signals are obtained using Welch's method [11] with a Hanning windowing function and 50% data overlap. The one-third octave bin-averaging technique is applied to smooth the sound spectra.

While primarily designed for aeroacoustic measurements, the A-Tunnel facility is also equipped with flow measurement techniques, including a Particle Image Velocimetry (PIV) system, as illustrated in Fig. 3(b). Planar PIV measurements were conducted using a LaVision Imager sCMOS CLHS camera at a frame rate of 15 Hz. These measurements aimed to capture flow fields within the LG wake region across three horizontal planes (i.e. $Z = 0$, $Z = 50$ mm and $Z = 120$ mm) and a vertical plane (i.e. $X = 170$ mm) (Fig. 4(b)). The field of view (FOV) for each plane is 180×240 mm^2. The resolution of the FOV is 24×24 pixels with a vector spacing of 0.6 mm. These flow and acoustic measurements are conducted at a flow velocity of 35 m/s. The details of experimental measurements can be found in Refs.[6, 8–10].

B. Numerical methods and simulation set-up

The simulations are performed utilizing the commercial finite-volume solver, STAR-CCM+, version 2021.1 [12]. The compressible Navier-Stokes equations are solved in a coupled manner. Convective fluxes are approximated using a bounded central difference scheme, which is a hybrid combining second-order upwind and central difference schemes. A second-order accurate scheme is applied for diffusive flux computation within interior grid cells. Time integration

employs an implicit, 2nd-order, three-level Euler scheme. For detailed information on the numerical algorithms, readers may refer to the STAR-CCM+ User Guide [13].

The dimensions of the three-dimensional (3D) computational domain in the streamwise (X), lateral (Y) and vertical (Z) directions are $130d_w$, $65d_w$ and $32.5d_w$, respectively. Figure 5 depicts a two-dimensional schematic of the computational domain with boundary conditions and an FW-H permeable integral surface. Apart from the inlet, outlet and slip wall, the remaining three boundaries of the 3D computational domain are free-stream boundaries. In the simulations, the LG axle is affixed to a slip wall in order to emulate the flat plate (Figure 3(a)) in the wind-tunnel measurements. In the present study, we simulate a baseline case and two controlled cases to investigate the noise-reduction capabilities of two diamond-lattice fairings (Figure 2). The detailed flow features around the baseline case are resolved with refined grids. For the controlled cases, rather than resolving the detailed flow through the fairings, a numerical model is employed to represent the fairing effect (Section II.C).

The computational meshes are generated using the STAR-CCM+ built-in mesh generator. The Polyhedral Mesher is adopted to generate polyhedral cells in the flow field. Near solid walls, the Advancing Layer Mesher is utilized to generate prism layers, ensuring that the first grid layer from the solid walls corresponds to a y^+ value of less than 1. The total numbers of grid cells in the simulations of the baseline LG and controlled LG are 73 and 87 million, respectively. Further information on the computational meshes, along with a grid sensitivity study on the baseline landing gear, can be found in Ref. [14].
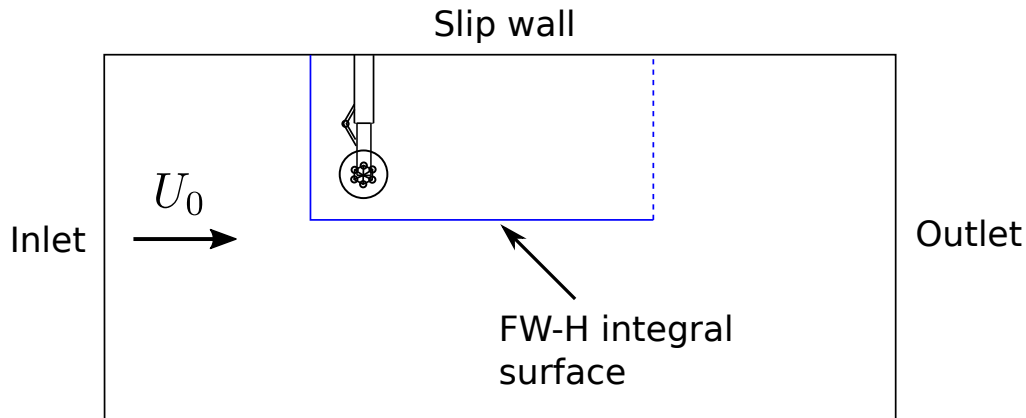

Fig. 5   A two-dimensional sketch of the computational domain with boundary conditions and an FW-H permeable integral surface.

The free-stream velocity is $U_0 = 35$ m/s with a low turbulence intensity of 0.1% and a turbulent viscosity ratio of 1.0 at the inlet boundary which gives the specific rate of dissipation ω. The Reynolds number, based on the free-stream velocity and the diameter of LG wheels, is $350,000$. A relatively small time step of $\Delta t = 1.0 \times 10^{-5}s$ is employed to advance the simulations. In the present numerical simulations, we will validate the predicted flow field by comparing the velocity statistics within a vertical plane ($X = 170$ mm), as well as along the wake center line ($Y = 0$) and a lateral line ($X = 255$ mm) within the three horizontal planes $Z = 0$, 50 mm and 120 mm, as illustrated in Figure 4(b). Far-field noise is computed by integrating noise sources on a permeable integral surface using the FW-H analogy. The permeable integral surface is designed as a box with an open downstream end in order to circumvent spurious noise generated by turbulent eddies passing through the downstream surface, as illustrated in Figure 5. Careful positioning ensures that the integral surface is sufficiently distant from the turbulent wake to encompass all noise sources, yet remains within the refined region to ensure ample grid resolution. The grid resolution used here enables a cut-off frequency of approximately 20 kHz.

C. Numerical modeling of diamond-lattice fairings

Similar to the modeling of other porous media [15–21], the model for diamond-lattice fairings incorporates a damping-type source term into the momentum equations. Specifically, within the fairing region, a source term S is
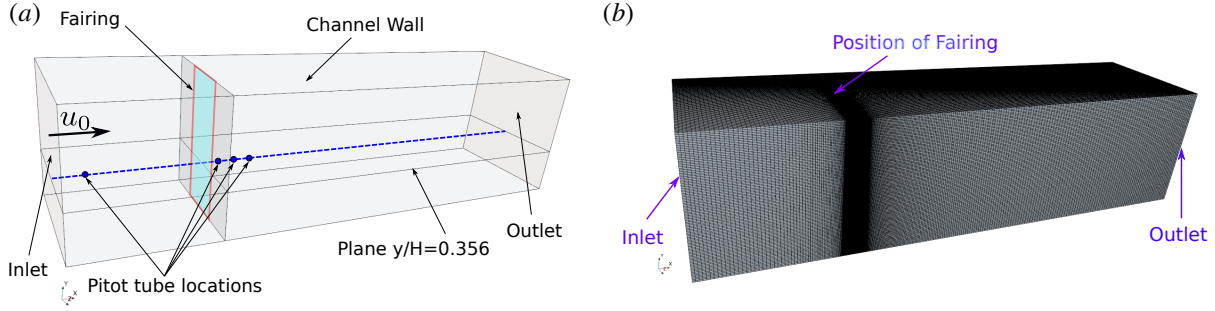
Fig. 6 Numerical setup: (a) A sketch illustrating the computational domain, with the blue dashed line marking the intersection of planes $y/H = 0.356$ and $z/H = 0.5$; and (b) a computational mesh (Mesh 2). Mean streamwise velocity, turbulence intensity and pressure drop were measured along the blue dashed line in the WAABLIEF wind tunnel [23].

introduced to the right-hand side (RHS) of the IDDES momentum equations, thus modifying the momentum equations as

$$\frac{\partial(\rho\hat{u}_i)}{\partial t} + \frac{\partial(\rho\hat{u}_i\hat{u}_j)}{\partial x_j} = -\frac{\partial\hat{p}}{\partial x_i} + \frac{\partial\hat{\sigma}_{ij}}{\partial x_j} + \frac{\partial\sigma_{ij,model}}{\partial x_j} + S_i, \tag{1}$$

where ρ is the fluid density, $\hat{u}_i$ is the components of velocity (i =1, 2, 3), $\hat{p}$ is the pressure, ' ˆ ' denotes Reynolds-averaging in the Reynolds-averaged Navier–Stokes (RANS) region and filtering in the large-eddy simulation (LES) region, respectively. $\hat{\sigma}_{ij}$ is the viscous stress tensor and $\sigma_{ij,model}$ is the modelled stress tensor.

If the airflow approaches the fairing at zero incident angle, the source term can be expressed as

$$\begin{bmatrix} S_1 \\ S_2 \\ S_3 \end{bmatrix} = \begin{bmatrix} -K_0 \times 0.5\rho\,|\hat{u}|\,\hat{u}/h \\ 0 \\ 0 \end{bmatrix}, \tag{2}$$

where $\hat{u}$ here is the streamwise velocity, h is the fairing thickness, and the resistance coefficient K_0 is 177.6 and 70.77 for DL 2.5mm and DL 4.5mm, respectively, as given by wind-tunnel measurements [22].

III. Validation of the diamond-lattice model

In this section, we validate the diamond-lattice model (Eq. (2)) against the recent measurements conducted in the Wind tunnel for AeroAcoustic Boundary Layer Including prEssure gradient eFfect (WAABLIEF) at the von Karman Institute for Fluid Dynamics (VKI) [23]. Figure 6(a) illustrates a sketch of the computational domain in the present large-eddy simulation of a channel flow. The computational domain is a meter-long channel with a square cross-section of 0.25 m × 0.25 m. The velocity at the channel inlet is u_0 = 16 m/s, corresponding to a Reynolds number of 132,000 based on the inlet velocity and the half-height of the channel. At the channel inlet, the velocity profile near the channel walls is prescribed according to the 1/7$^{\text{th}}$ power law [24]. Similar to the WAABLIEF experiments [23], in numerical simulations, the diamond-lattice fairings have a width of L = 0.054 m and a height of H = 0.25 m. Figure 6(b) displays one of the computational meshes generated by the 'Direct Mesh' tool in STAR-CCM+. The computational domain is partitioned into upstream and downstream blocks, separated at the location of the fairing. The mesh is then generated by controlling the size at two edges of the upstream and downstream blocks as well as the number of cells in each block. By varying the cell size at the position of the fairing, three different meshes are generated and tested (Table 1).

Utilizing the fairing model described by Eq. (2), Figure 7 shows the mean streamwise velocity and turbulent intensity [25] along the line intersecting planes y/H = 0.356 and z/H = 0.5 for the DL 4.5mm fairing. In the mean streamwise velocity profile, a short plateau is observed downstream from the fairing extending to a distance of L. Then, the mean streamwise velocity decreases to a minimum value at x/L = 6.7. The simulations exhibit a slight over-prediction compared to the experimental data. Regarding turbulent intensity, the simulations follow a similar trend to the experimental data, albeit with a steeper slope. Figure 8 illustrates the pressure drop, showing good agreement

6

Table 1   Computational meshes for channel-flow simulations.

Mesh	Δx_{min} (mm)	$\Delta x_{max,u}$ (mm)	$\Delta x_{max,d}$ (mm)	Δy^a (mm)	Δz (mm)	# cells (million)
1	1.0	5.0	5.0	2.7	2.7	6.4
2	0.042	5.0	5.0	2.7	2.7	6.4
3	0.0084	6.0	7.0	2.7	2.7	8.0

$^a\Delta y$ listed here is for cells away from the channel walls. In the near-wall regions, the meshes include prism layers with $y^+ < 1$. The same goes for Δz as well.

between numerical predictions and experimental measurements [23] at three locations in the downstream of the fairing, i.e. $(x - x_{fairing})/L = 0.185$, 0.741 and 1.296. As per Zamponi et al. [25], the turbulent intensity is defined as

$$U' = \sqrt{(u' \cos \alpha)^2 + (v' \cos \alpha)^2}, \tag{3}$$

where α is

$$\alpha = \tan^{-1}\left(\frac{\bar{v}}{\bar{u}}\right). \tag{4}$$

This is a result of the fact that, for low turbulence levels, a single normal hot-wire only responds to fluctuations in the direction of the mean velocity [25].
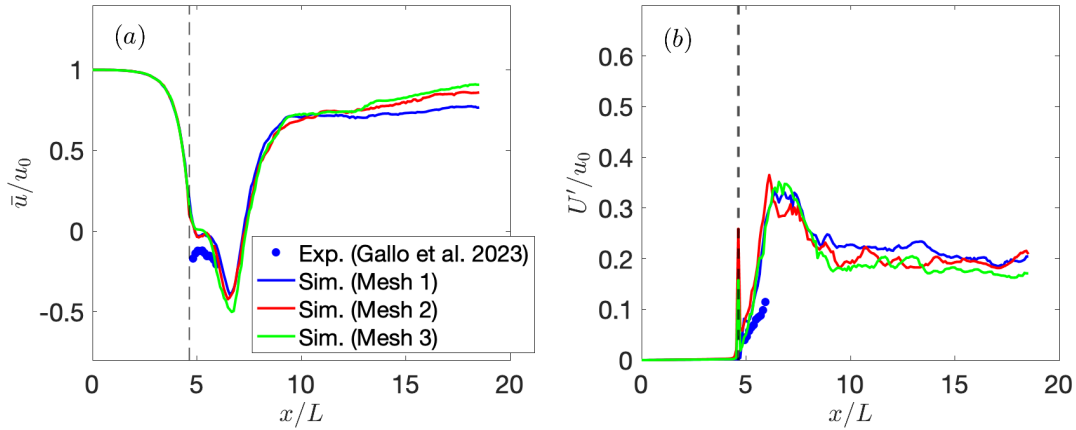

Fig. 7   Flow statistics along the line at the intersection of planes $y/H = 0.356$ **and** $z/H = 0.5$**: (**a**) Mean streamwise velocity; (**b**) turbulent intensity. In the simulations, the fairing model in Eq. (2) is applied and tested on three different meshes. The black dashed lines indicate the position of the DL 4.5mm fairing, i.e.** $x/L = 4.63$**.**

IV. Results on landing gears

In this section, we present the flow and acoustic results for the baseline configuration, along with those of the two controlled configurations equipped with diamond-lattice fairings.

Figures 9 and 10 present the contours of mean flow velocities and root-mean-square velocity fluctuations in the vertical plane located in the turbulent wake, at $X = 170$ mm, for the baseline configuration and the DL 2.5mm configuration, respectively. Overall, good agreement between the IDDES simulations and the PIV measurements is observed. Figure 11 shows the contours of mean flow velocities and root-mean-square velocity fluctuations in the same plane for the DL 4.5mm configuration. The PIV measurement is not conducted for this configuration and hence is not shown here. Quantitative comparisons of the flow statistics between the IDDES simulations and the PIV measurements in the LG wake are shown in Figures 12-14.

Figure 12 illustrates the pressure distribution (C_p) on the left wheel and the rod at $Z = 50$ mm, as predicted in the simulations and measured in the experiments. On the wheel surface, notable agreement between numerical predictions
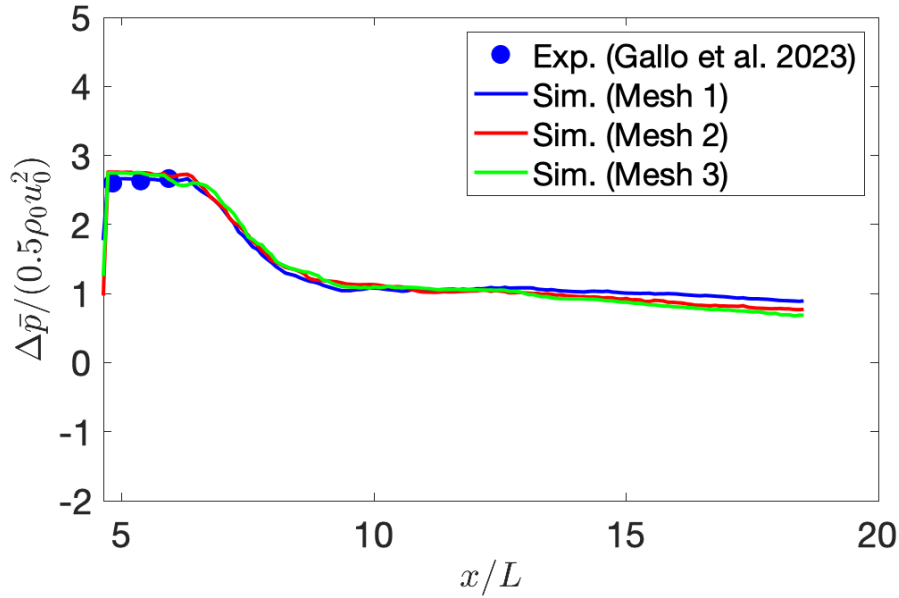
Fig. 8 Pressure drop along the line at the intersection of planes $y/H = 0.356$ **and** $z/H = 0.5$**. In the simulations, the fairing model in Eq. (2) is applied and tested on three different meshes. The diamond-lattice fairing is located at** $x/L = 4.63$**, i.e. the** y**-axis.**

and experimental data is observed. However, on the rod surface, while the predicted pressure coefficient in the controlled cases aligns well with experimental one, a disparity arises for the baseline case, particularly between 80° and 120° where boundary layer separation occurs [26]. Additionally, the numerical simulation tends to underestimate the pressure coefficient at $\theta > 140°$ on the rear side of the rod. These inconsistencies likely stem from differences in local Reynolds numbers between the simulation and experiment, influencing boundary layer separation and subsequently, the pressure distribution. Furthermore, in both controlled cases, C_p remains relatively constant along the rod, indicating minimal flow impingement in the low-speed flow region behind the fairing. Consequently, the fairing acts as a shielder for the rod and torque link, diminishing noise generation. This noise-reduction effect through shielding was also observed by Zhao et al. [5].

Figure 13 presents a comparison of predicted flow statistics along the wake centerline with PIV experiments for the baseline and both controlled cases. Generally, good agreement is observed between the numerical predictions and experiments for both the mean streamwise velocity and the root-mean-square of the streamwise velocity fluctuation, except at $Z = 120$ mm for the baseline case (Figure 13(e) and (f)). The discrepancy at Z = 120 mm in the baseline case is likely attributable to two factors: (i) the intricate geometry of the torque link, which generates much finer-scale turbulence, and (ii) the complexity of the joint downstream of the torque link between the larger and smaller rods, where precise numerical prediction is challenging. Resolving these complexities and small-scale turbulence demands a much finer mesh. However, as demonstrated in the subsequent acoustic analysis, this discrepancy does not significantly impact noise prediction.

Figure 14 depicts the predicted flow statistics along the vertical line at $X = 255$ mm in comparison with PIV measurements. The most significant deviation occurs at $Y = 0$ for the baseline case (Fig. 14(e)), corresponding to the discrepancy shown in Fig. 13(e). However, as the distance from $Y = 0$ increases, the deviation diminishes. Overall, there is good agreement between the numerical simulation and the experiments. Notably, the agreement for the two controlled cases is generally better than that for the baseline case, indicating that simulating the baseline case is more challenging. This difficulty likely arises from the complex turbulent wakes generated by the torque link and the intricate joint downstream of the torque link between the larger and smaller rods. In contrast, these flow features are absent in the controlled cases due to the shielding effect of the diamond-lattice fairings.

The sound pressure level (SPL) distributed on the surface of the landing gear with and without fairings is illustrated in Figure 15. In this representation, the SPL is the logarithmic value of the ratio between the root-mean-square surface
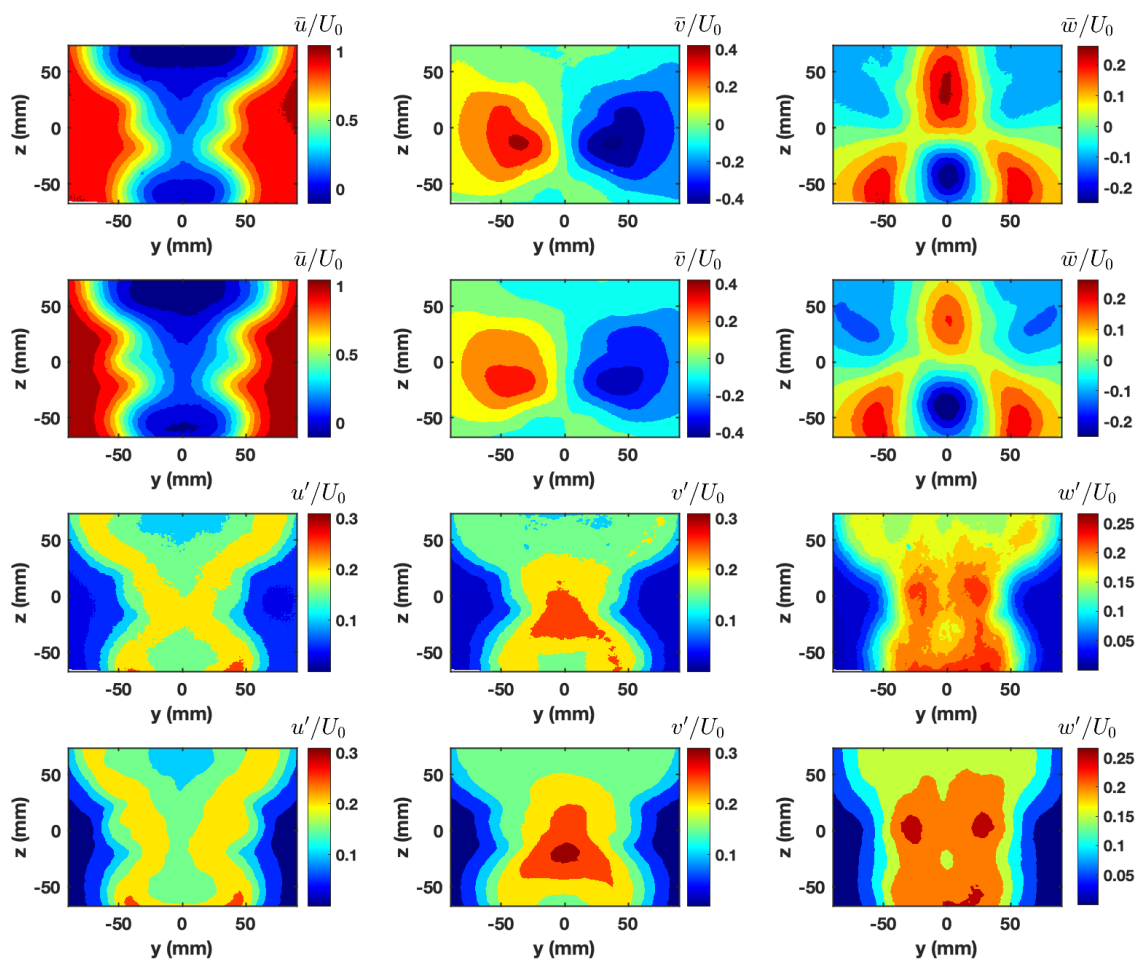
8

Fig. 9 **Comparison of mean velocities and root-mean-square velocity fluctuations in plane** $X = 170$ **mm between IDDES simulation and PIV measurement in the baseline LG configuration. First and third rows: PIV; second and fourth rows: IDDES.**
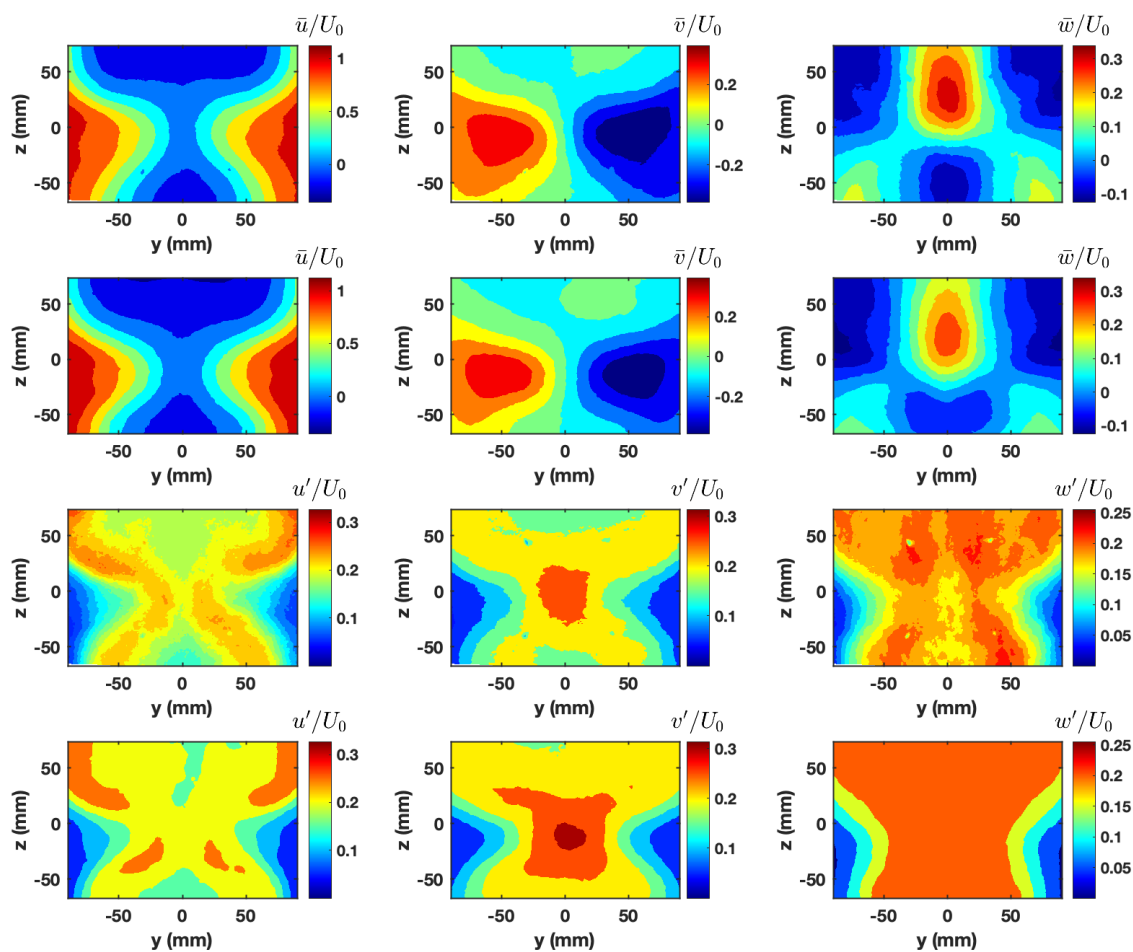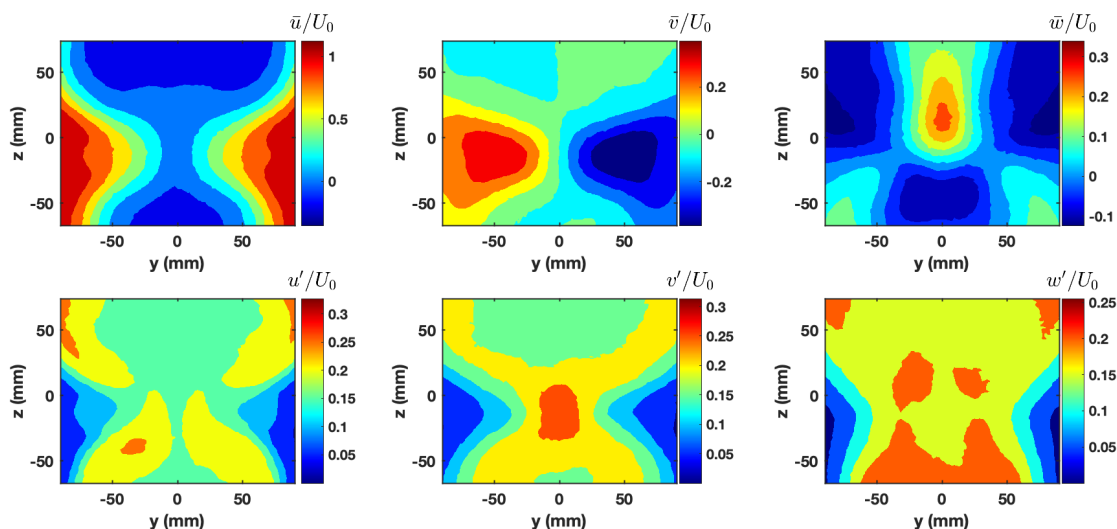
9

Fig. 10   Comparison of mean velocities and root-mean-square velocity fluctuations in plane $X = 170$ mm between IDDES simulation and PIV measurement of the DL 2.5mm configuration. First and third rows: PIV; second and fourth rows: IDDES.

Fig. 11   Mean velocities and root-mean-square velocity fluctuations in plane $X = 170$ mm in the IDDES simulation of the DL 4.5mm configuration. In this study, PIV measurement is not conducted for this configuration.
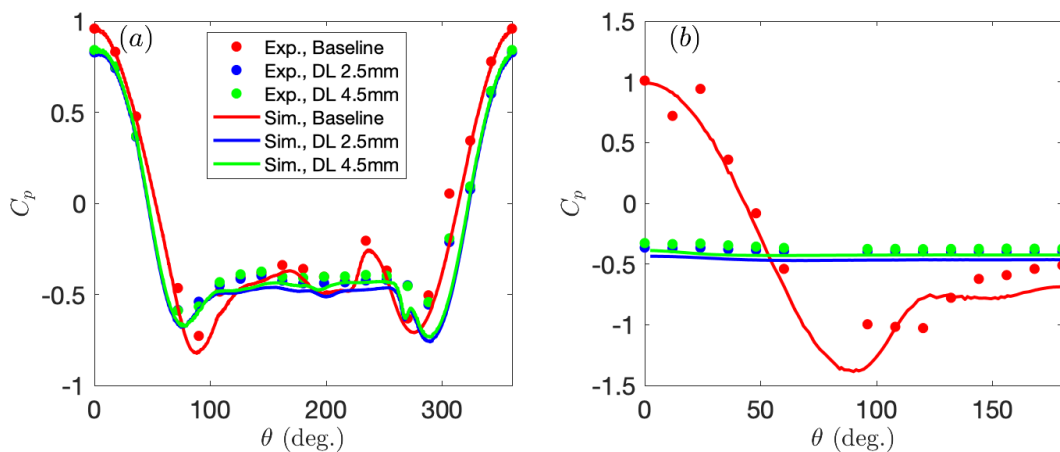

Fig. 12   Comparison of the pressure coefficients on the surfaces of an LG wheel and a rod in the three LG configurations: (*a*) **Wheel;** (*b*) **rod at** $Z = 50$ **mm.**
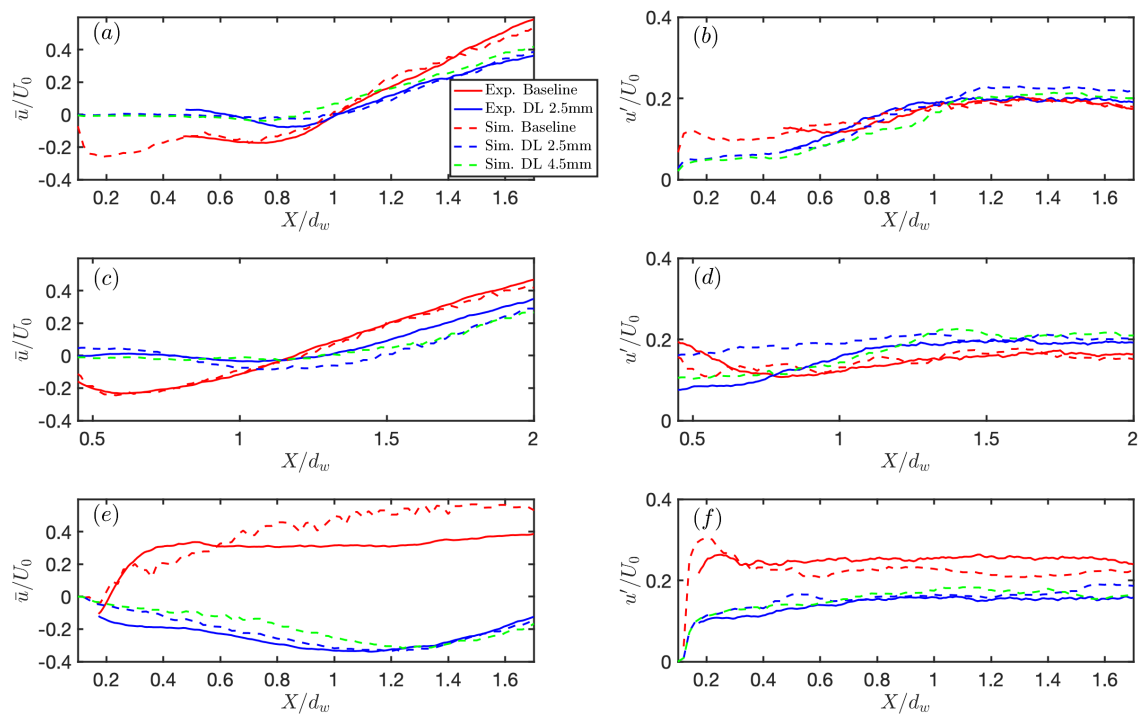
11

Fig. 13 **Flow statistics along the wake center lines in the three LG configurations:** (*a*) **Mean streamwise velocity at** $Z = 0$**;** (*b*) **root-mean-square of streamwise velocity fluctuation at** $Z = 0$**;** (*c*) **mean streamwise velocity at** $Z = 50$ **mm;** (*d*) **root-mean-square of streamwise velocity fluctuation at** $Z = 50$ **mm;** (*e*) **mean streamwise velocity at** $Z = 120$ **mm;** (*f*) **root-mean-square of streamwise velocity fluctuation at** $Z = 120$ **mm.**
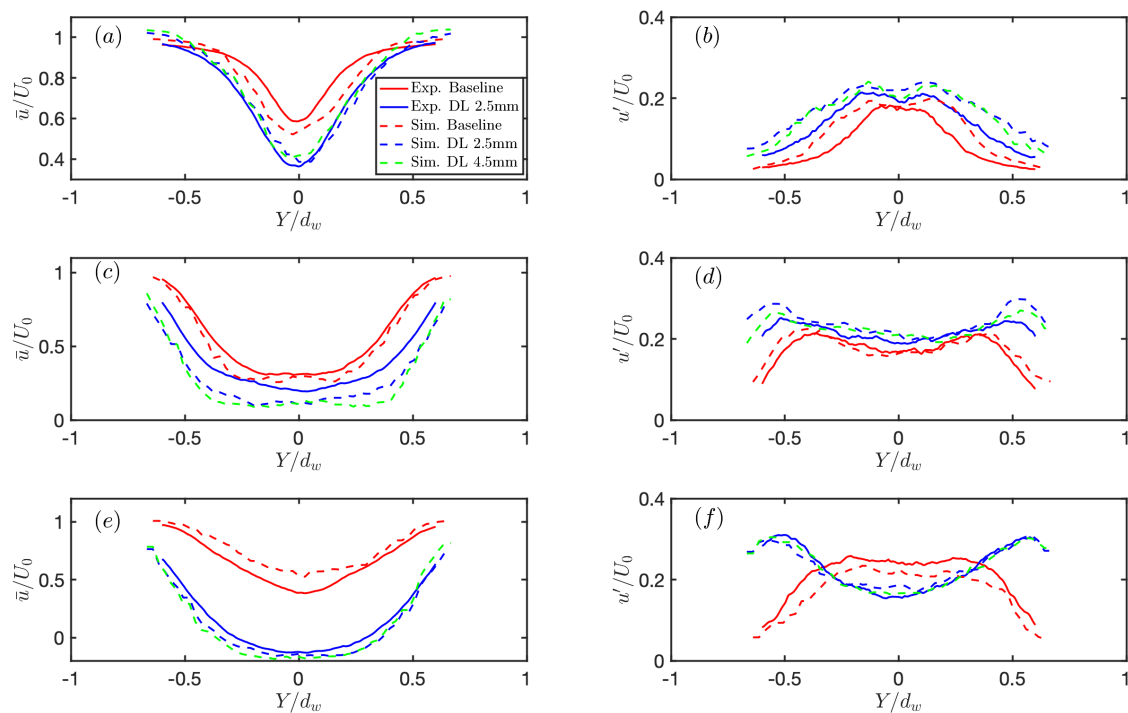
Fig. 14   Flow statistics along the wake vertical lines at $X = 255$ **mm in the three LG configurations:** (*a*) **Mean streamwise velocity at** $Z = 0$**;** (*b*) **root-mean-square of streamwise velocity fluctuation at** $Z = 0$**;** (*c*) **mean streamwise velocity at** $Z = 50$ **mm;** (*d*) **root-mean-square of streamwise velocity fluctuation at** $Z = 50$ **mm;** (*e*) **mean streamwise velocity at** $Z = 120$ **mm;** (*f*) **root-mean-square of streamwise velocity fluctuation at** $Z = 120$ **mm.**
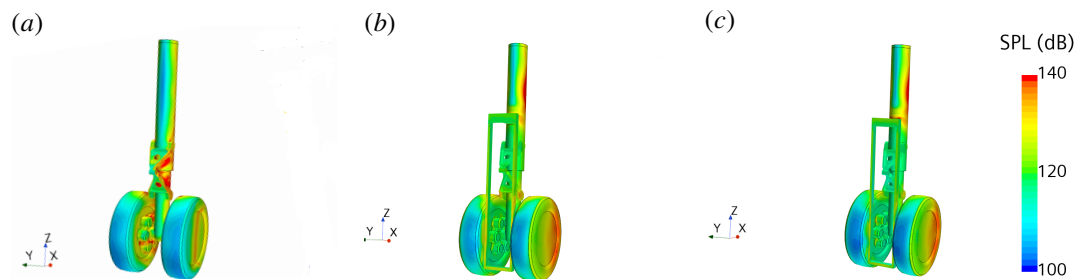

Fig. 15   Sound pressure level distributed on the surface of the landing gears: (*a*) **Baseline case;** (*b*) **controlled case with the DL 4.5mm fairing; and** (*c*) **controlled case with the DL 2.5mm fairing.**
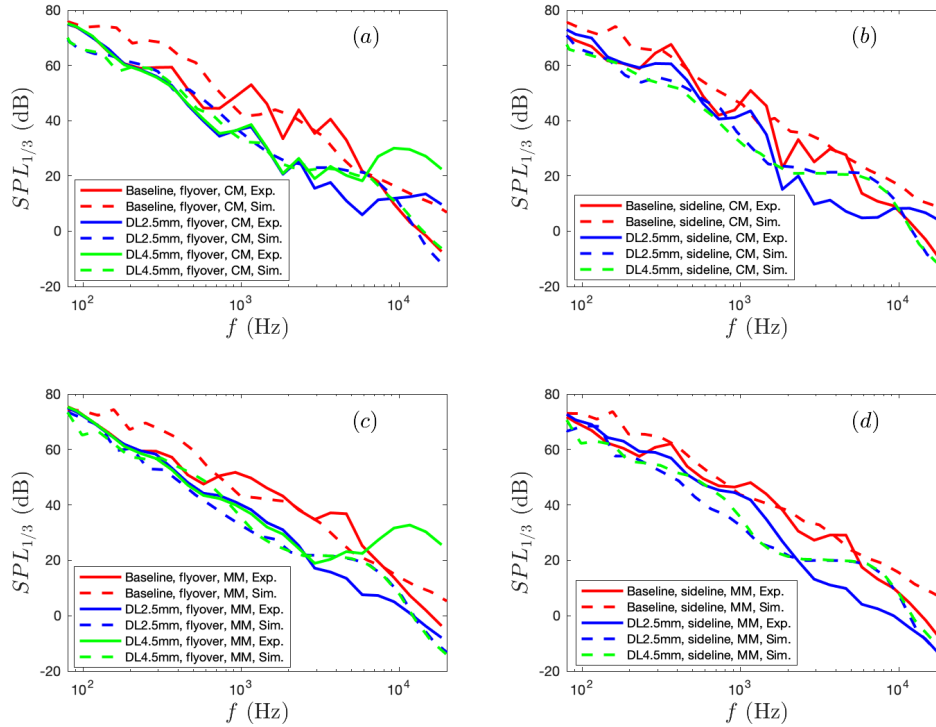
13

Fig. 16   The 1/3-octave bin-averaged SPL of the FW-H predictions and microphone measurements in the three LG configurations: (*a*) **Center microphone of the flyover array;** (*b*) **center microphone of the sideline array;** (*c*) **mean of the flyover 64-microphone array;** (*d*) **mean of the sideline 64-microphone array.**

pressure fluctuation (p'_{rms}) and the reference pressure ($p_{ref} = 20\mu$Pa), as follows

$$SPL = 20 \log \left(\frac{p'_{rms}}{p_{ref}} \right).$$ (5)

In the baseline LG configuration, both the torque link and the brakes are significant noise sources, as evidenced by the high-level SPL distribution on the the brakes and the higher-level SPL distribution on the torque link in Figure 15(a). Introducing either of the diamond-lattice fairings results in reduced noise levels on both the torque link and the brakes. Consequently, the fairing acts as a shielder for these components, attenuating the pressure fluctuations distributed on them. However, it is worth noting that the shielding effect of the fairings also leads to a redistribution of noise sources. This redistribution is evident in Figure 15(b) and (c), where a noise source shifts to the upper part of the landing gear rod. This shift occurs due to the redirection of flow caused by the fairings' shielding effect.

Figure 16 displays the 1/3-octave bin-averaged SPL for both flyover and sideline configurations, presenting experimental and numerical results for both the center microphone and the average of the microphone array. It should be noted that the measurement of the DL 4.5mm fairing in the sideline configuration is not performed in this study and hence the data is missing here. In the baseline case, there is satisfactory agreement between the measurements and the numerical predictions, particularly in the middle-frequency range. However, for the two controlled cases, while the numerical predictions align well with the experiments in the low-to-middle frequency range, deviations occur from 4000 Hz onwards (although for the DL 2.5mm fairing, agreement with the experiment is reestablished from 10000 Hz). Firstly, for the DL 4.5mm fairing, there is an upward trend of the experimental SPL at high frequencies, possibly due to pore-scale turbulent flows inside the pores. Since the simulations did not resolve the detailed flow features within the porous fairings, such noise could not be predicted using the employed diamond-lattice models. Secondly, the deviation could result from inaccuracies in resolving flow features at the small gaps (with a dimension of 0.5 mm) between the fairing and the LG wheels, as estimated by the Strouhal number. Overall, it is evident that the installation of
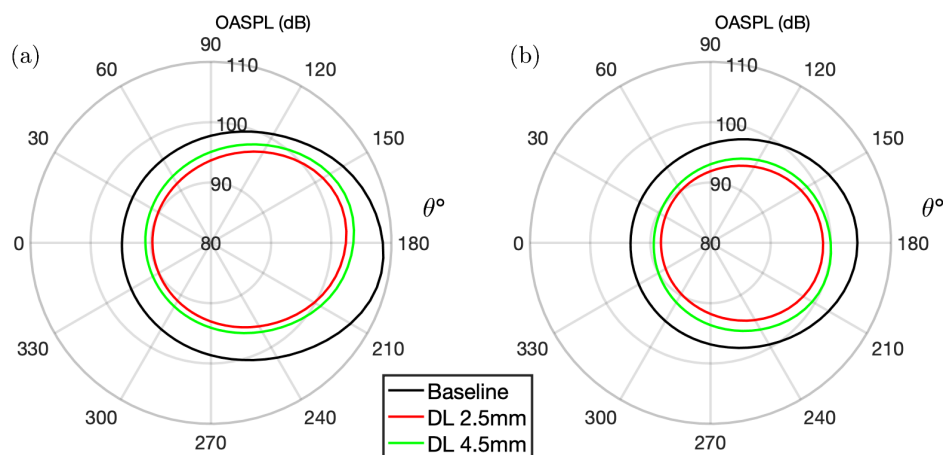
14

Fig. 17   Comparison of OASPL directivity for the simulated baseline and controlled LAGOON-like landing gears: (*a*) **Circle on plane** $Y = 0$ **with a radius of 1.05 m;** (*b*) **circle on plane** $Z = 0$ **with a radius of 1.36 m.**

a diamond-lattice fairing upstream of the landing gear effectively reduces LG noise. Figure 17 provides a comparison of the directivity of the overall sound pressure level (OASPL) for the three simulated configurations. In comparison to the baseline case, the DL 4.5mm fairing yields a noise reduction of 2-6 dB across all radial directions. The DL 2.5mm fairing proves more effective, resulting in a noise reduction of 3-7 dB across all radial directions.

V. Concluding remarks

In this paper, we conduct numerical and experimental investigations into the noise-reduction effectiveness of two passive add-on porous fairings that are comprised of diamond grids measuring 2.5 mm and 4.5 mm in size, respectively. The turbulent flows over a baseline landing gear, a modified version of the LAGOON landing gear with its inner rim cavities closed, along with two configurations equipped with diamond-lattice fairings, are simulated using IDDES in combination with the FW-H analogy for acoustic analysis. Instead of resolving the detailed flow features through the diamond-lattice fairings, a numerical model is used to represent the effect of fairing. Prior to applying the numerical model in the simulations of flow past landing gears, rigorous validation of the fairing model against experimental data in a channel flow is performed. Subsequently, flow and acoustic quantities in the LG simulations are respectively compared to PIV and microphone measurements conducted at the anechoic A-Tunnel of Delft University of Technology. Overall, reasonable agreement between the numerical prediction and the experiment is observed. Results show that far-field noise in the frequency range beyond 200 Hz can be effectively reduced through the installation of a diamond-lattice fairing upstream of the landing gear. For the baseline landing gear, the torque link and the brakes are potent noise sources. Both diamond-lattice fairings mitigate the pressure fluctuation on the torque link and brakes, resulting in the reduction of surface noise sources. The noise directivity shows that the DL 4.5mm fairing produces a noise reduction of 2-6 dB whereas the DL 2.5mm fairing generates a noise reduction of 3-7 dB across all radial directions.

Overall, both diamond-lattice fairings are effective in mitigating landing gear noise. Furthermore, the present numerical approach represents a valuable modeling method to support effective design and optimization of fairings dedicated to next-generation quieter aircraft landing gears.

Acknowledgments

15

References

[1] Dobrzynski, W., Ewert, R., Pott-Pollenske, M., Herr, M., and Delfs, J., "Research at DLR towards airframe noise prediction and reduction," *Aerospace Science and Technology*, Vol. 12, No. 1, 2008, pp. 80–90.

[2] Piet, J. F., Davy, R., Elias, G., Siller, H., Chow, L., Seror, C., and Laporte, F., "Flight test investigation of add-on treatments to reduce aircraft airframe noise," *11th AIAA/CEAS aeroacoustics conference*, 2005, p. 3007.

[3] Boorsma, K., Zhang, X., and Molin, N., "Perforated fairings for bluff body noise control," *13th AIAA/CEAS Aeroacoustics Conference (28th AIAA Aeroacoustics Conference)*, 2007, p. 3462.

[4] Boorsma, K., Zhang, X., and Molin, N., "Landing gear noise control using perforated fairings," *Acta Mechanica Sinica*, Vol. 26, 2010, pp. 159–174.

[5] Zhao, K., Okolo, P., Neri, E., Chen, P., Kennedy, J., and Bennett, G. J., "Noise reduction technologies for aircraft landing gear-A bibliographic review," *Progress in Aerospace Sciences*, Vol. 112, 2020, p. 100589.

[6] Bennett, G. J., Lai, J., O'Brien, G., Ragni, D., Avallone, F., and Pott-Pollenske, M., "Flow Control and Passive Low Noise Technologies for Landing Gear Noise Reduction," *28th AIAA/CEAS Aeroacoustics 2022 Conference*, 2022, p. 2848.

[7] Casalino, D., Ribeiro, A. F., Fares, E., and Nölting, S., "Lattice–Boltzmann aeroacoustic analysis of the LAGOON landing-gear configuration," *AIAA journal*, Vol. 52, No. 6, 2014, pp. 1232–1248.

[8] Merino-Martínez, R., Carpio, A. R., Pereira, L. T. L., van Herk, S., Avallone, F., Ragni, D., and Kotsonis, M., "Aeroacoustic design and characterization of the 3D-printed, open-jet, anechoic wind tunnel of Delft University of Technology," *Applied Acoustics*, Vol. 170, 2020, p. 107504.

[9] Gondrum, M., Niemöller, A., Meinke, M., Schroeder, W., Rubio Carpio, A., Ragni, D., and Avallone, F., "Landing gear noise mitigation by an upstream installed fairing," *28th AIAA/CEAS Aeroacoustics 2022 Conference*, 2022, p. 2847.

[10] Terracol, M., Manoha, E., Manueco, L., Avallone, F., Ragni, D., and Rubio Carpio, A., "Numerical Simulations of a Landing Gear with Flow Through Fairings for Noise Mitigation," *AIAA AVIATION 2023 Forum*, 2023, p. 4173.

[11] Welch, P., "The use of fast Fourier transform for the estimation of power spectra: a method based on time averaging over short, modified periodograms," *IEEE Transactions on audio and electroacoustics*, Vol. 15, No. 2, 1967, pp. 70–73.

[12] Siemens Digital Industries Software, "Simcenter STAR-CCM+, version 2021.1," , Siemens 2021.

[13] Siemens Digital Industries Software, "Simcenter STAR-CCM+ User Guide v. 2021.1," , Siemens 2021.

[14] Li, S., Davidson, L., Peng, S.-H., Rubio Carpio, A., Ragni, D., Avallone, F., and Koutsoukos, A., "On the mitigation of landing gear noise using a solid fairing and a dense wire mesh," *under review*, 2024.

[15] Teruna, C., Manegar, F. A., Avallone, F., Casalino, D., Ragni, D., Rubio Carpio, A., and Carolus, T., "Numerical analysis of metal-foam application for trailing edge noise reduction," *25th AIAA/CEAS Aeroacoustics Conference*, 2019, p. 2650.

[16] Teruna, C., Manegar, F., Avallone, F., Ragni, D., Casalino, D., and Carolus, T., "Noise reduction mechanisms of an open-cell metal-foam trailing edge," *Journal of Fluid Mechanics*, Vol. 898, 2020.

[17] Teruna, C., Rego, L., Avallone, F., Ragni, D., and Casalino, D., "Applications of the Multilayer Porous Medium Modeling Approach for Noise Mitigation," *Journal of Aerospace Engineering*, Vol. 34, No. 6, 2021, p. 04021074.

[18] Okolo, P. N., Zhao, K., Kennedy, J., and Bennett, G. J., "Mesh screen application for noise reduction of landing gear strut," *22nd AIAA/CEAS Aeroacoustics Conference*, 2016, p. 2845.

[19] Okolo, P. N., Zhao, K., Kennedy, J., and Bennett, G. J., "Numerical modeling of wire screens for flow and noise control," *23rd AIAA/CEAS Aeroacoustics Conference*, 2017, p. 3700.

16

[20] Li, S., Davidson, L., and Peng, S.-H., "Numerical modeling of a wire mesh for aerodynamic noise reduction," *Physics of Fluids*, Vol. 35, No. 1, 2023, p. 015103.

[21] Li, S., Davidson, L., and Peng, S.-H., "A pressure-loss model for flow-through round-hole perforated plates of moderate porosity and thickness in laminar and turbulent flow regimes," *International Journal of Heat and Mass Transfer*, Vol. 226, 2024, p. 125490.

[22] Méry, F., and Sebbane, D., "Aerodynamic characterisation of porous fairings: pressure drop and Laser Doppler Velocimetry measurements," *Scientific Data*, Vol. 10, No. 1, 2023, p. 39.

[23] Gallo, E., Zamponi, R., Zarri, A., Kucukosman, Y. C., and Schram, C. F., "Experimental Characterization of Flow Through Porous Fairings," *AIAA AVIATION 2023 Forum*, 2023, p. 4175.

[24] Van de Wyer, N., Zapata, A., Nogueira, D., and Schram, C. F., "Development of a test rig for the measurement of turbulent boundary layer wall pressure statistics," *2018 AIAA/CEAS Aeroacoustics Conference*, 2018, p. 3122.

[25] Zamponi, R., Satcunanathan, S., Moreau, S., Ragni, D., Meinke, M., Schröder, W., and Schram, C., "On the role of turbulence distortion on leading-edge noise reduction by means of porosity," *Journal of Sound and Vibration*, Vol. 485, 2020, p. 115561.

[26] Li, S., Rival, D. E., and Wu, X., "Sound source and pseudo-sound in the near field of a circular cylinder in subsonic conditions," *Journal of Fluid Mechanics*, Vol. 919, 2021, p. A43.